Energetics and Cooperativity of Tertiary Hydrogen Bonds in RNA Structure[†]

Scott K. Silverman* and Thomas R. Cech*

Howard Hughes Medical Institute and Department of Chemistry and Biochemistry, Campus Box 215, University of Colorado at Boulder, Boulder, Colorado 80309-0215

Received March 17, 1999; Revised Manuscript Received April 30, 1999

ABSTRACT: Tertiary interactions that allow RNA to fold into intricate three-dimensional structures are being identified, but little is known about the thermodynamics of individual interactions. Here we quantify the tertiary structure contributions of individual hydrogen bonds in a "ribose zipper" motif of the recently crystallized *Tetrahymena* group I intron P4−P6 domain. The 2′-hydroxyls of P4−P6 nucleotides C109/A184 and A183/G110 participate in forming the "teeth" of the zipper. These four nucleotides were substituted in all combinations with their 2′-deoxy and (separately) 2′-methoxy analogues, and thermodynamic effects on the tertiary folding $\Delta G^{\circ\prime}$ were assayed by the Mg^{2+} dependence of electrophoretic mobility in nondenaturing gels. The 2′-deoxy series showed a consistent trend with an average contribution to the tertiary folding $\Delta G^{\circ\prime}$ of −0.4 to −0.5 kcal/mol per hydrogen bond. Contributions were approximately additive, reflecting no cooperativity among the hydrogen bonds. Each "tooth" of the ribose zipper (comprising two hydrogen bonds) thus contributes about −1.0 kcal/mol to the tertiary folding $\Delta G^{\circ\prime}$. Single 2′-methoxy substitutions destabilized folding by ∼1 kcal/mol, but the trend reversed with multiple 2′-methoxy substitutions; the folding $\Delta G^{\circ\prime}$ for the quadruple 2′-methoxy derivative was approximately unchanged relative to wild-type. On the basis of these data and on temperature-gradient gel results, we conclude that entropically favorable hydrophobic interactions balance enthalpically unfavorable hydrogen bond deletions and steric clashes for multiple 2′-methoxy substitutions. Because many of the 2′-deoxy derivatives no longer have the characteristic hydrogen-bond patterns of the ribose zipper motif but simply have individual long-range ribose-base or ribose-ribose hydrogen bonds, we speculate that the energetic value of −0.4 to −0.5 kcal/mol per tertiary hydrogen bond may be more generally applicable to RNA folding.

Many RNA molecules rely on a specific three-dimensional structure for their biological activity. RNA structure is stabilized by both secondary and tertiary elements. Numerous thermodynamic measurements of RNA secondary structure (base-paired helices and hairpin loops) have been made, and in general, the understanding of RNA secondary structure is mature (*1*). However, exploration of RNA tertiary structure energetics is in its infancy. Many tertiary contacts have been identified at atomic resolution by X-ray crystallography or by NMR spectroscopy but not analyzed thermodynamically (*2*−*5*). Conversely, several RNA tertiary interactions have been quantified energetically but not viewed at atomic resolution, so it is unclear how many hydrogen bonds or other contacts are involved (*6*−*11*). Here we dissect the thermodynamics of the "ribose zipper" motif, a set of tertiary contacts that has been observed in the X-ray crystal structures of the *Tetrahymena* group I intron P4−P6[1] domain (*3*) and the hepatitis delta virus (HDV) ribozyme (*4*), as well as in intermolecular contacts of the crystallized hammerhead ribozyme (*5*, *12*).

The "ribose zipper" is a recurring RNA structural motif comprising a specific array of hydrogen bonds. The 2′-hydroxyl of one nucleotide (partner I) donates a hydrogen bond to the 2′-hydroxyl of a second nucleotide (partner II), which in turn donates a hydrogen bond to the base of partner I (Figure 1). We view each such pair of hydrogen bonds as contributing one "tooth" to the overall "zipper" motif. In the structure of the 160-nucleotide P4−P6 domain, five teeth are found and in two places pairs of teeth are adjacent, prompting the analogy to a zipper (*3*).

In this study, we examined two adjacent ribose zipper teeth in P4−P6: the C109/A184 and A183/G110 interactions (Figure 1). We substituted these nucleotides with their 2′-deoxy or 2′-methoxy analogues (30 mutants total) and examined the energetic effects on tertiary folding with a quantitative Mg^{2+}-dependent nondenaturing-gel assay. Because we used the P4−P6 X-ray crystal structure as a guide to target individual tertiary interactions, we were hopeful that the resulting thermodynamic perturbations could be interpreted in terms of local modifications, instead of global changes in folding. Indeed, we feel that our data justify such interpretation, as will be described.

[†] This work was supported by Grant GM28039 from the National Institutes of Health. S.K.S. was supported by an American Cancer Society postdoctoral fellowship and is a fellow of the Helen Hay Whitney Foundation. T.R.C. is an Investigator of the Howard Hughes Medical Institute and an American Cancer Society Professor.

* To whom correspondence should be addressed. (S.K.S.) Phone: (303) 492-5607. Fax: (303) 492-6194. E-mail: Scott.Silverman@colorado.edu. (T.R.C.) (303) 492-8606.

[1] Abbreviations: P4−P6, the P4−P6 domain of the *Tetrahymena* group I intron RNA; P4−P6-bp, the J5/5a-base-paired mutant of P4−P6; PAGE, polyacrylamide gel electrophoresis; TGGE, temperature gradient gel electrophoresis; Tris, tris(hydroxymethyl)aminomethane; EDTA, ethylenediaminetetraacetic acid; TEMED, *N*,*N*,*N*′,*N*′-tetramethylethylenediamine.

10.1021/bi9906118 CCC: $18.00
Published on Web 06/17/1999

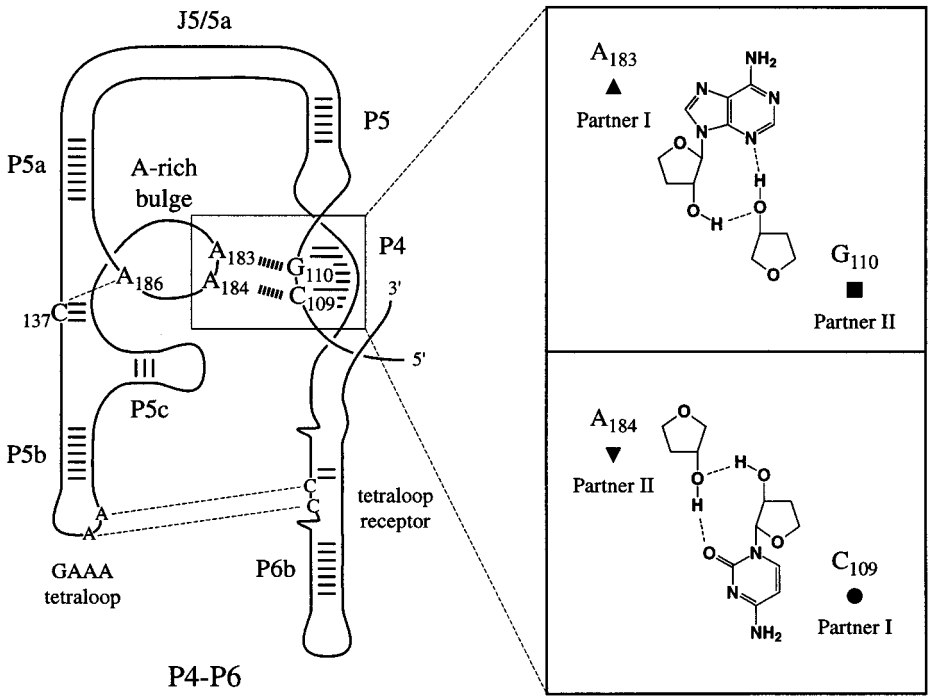

FIGURE 1: Ribose zipper motifs in P4−P6. The motif is illustrated on the right for two of the five ribose zipper "teeth" observed in the P4−P6 crystal structure, C109/A184 and A183/G110. Note that a 2′-deoxy substitution at partner I disrupts one hydrogen bond, while a 2′-deoxy substitution at partner II deletes two hydrogen bonds. In contrast, a 2′-methoxy substitution at either partner should disrupt only one hydrogen bond. Other ribose zipper teeth in P4−P6 are at C137/A186 in the A-rich bulge and at two other positions in the tetraloop/receptor. The geometric symbols shown in the boxes on the right are the same ones used in Figure 3 to indicate sites of 2′-substitution.

Two questions are addressed. (1) Quantitatively, how strong are these intramolecular tertiary structure hydrogen bonds? (2) Are these ribose zipper interactions cooperative or independent? Our results indicate that for the particular interactions studied, the hydrogen bonds each contribute about −0.4 to −0.5 kcal/mol to the tertiary folding $\Delta G^{\circ\prime}$ of P4−P6. Furthermore, we find that the hydrogen bonds composing the ribose zipper contribute approximately additively to the folding $\Delta G^{\circ\prime}$. Thus, the "zipper" analogy should not be taken to imply cooperativity between the adjacent "teeth" that form each zipper. Because the value of −0.4 to −0.5 kcal/mol per tertiary hydrogen bond also pertains to the P4−P6 derivatives in which intact ribose zipper interactions are replaced with simple long-range ribose−base or ribose−ribose hydrogen bonds, we speculate that this energetic value may be characteristic of simple pairwise long-range interactions that mediate higher-order RNA folding.

MATERIALS AND METHODS

Cloning, RNA Preparation, and Radiolabeling. The wild-type P4−P6 construct was the natural sequence previously reported (*3*) in a plasmid derived from the pTZL-21 construct (*13*). The J5/5a-base-paired mutant of P4−P6 (P4−P6-bp) was also as previously reported (*14*) in the pUC19 vector. Wild-type P4−P6 and P4−P6-bp plasmids were linearized with *Ear*I. RNA was transcribed in vitro using T7 RNA polymerase prepared by Anne Gooding in the Cech lab. Transcription conditions for P4−P6: 20 μg/mL linearized plasmid DNA, 40 mM Tris, pH 8.0, 40 mM DTT, 30 mM $MgCl_2$, 4 mM each NTP, and 2 mM spermidine, 25 °C, 15−20 h. RNA was purified by PAGE. Gels were prepared with 1× TBE buffer (89 mM Tris, 89 mM boric acid, pH ∼8.5, and 2 mM EDTA), 7 M urea, and 6% acrylamide:bisacrylamide (29:1, Fisher 40% stock), polymerized by addition of 1/200 by volume of 10% ammonium persulfate and 1/2000 by volume of TEMED; running buffer was 1× TBE. Bands were identified by UV shadowing, crushed with a glass rod, and extracted twice with TEN (10 mM Tris, pH 8.0, 1 mM EDTA, and 300 mM NaCl). RNA was isolated by precipitation with 3 vol of ethanol at −20 °C and centrifugation. RNA was quantified by UV absorbance (A_{260}) at room temperature using ϵ_{260} values calculated from the base composition with extinction coefficients ϵ (10^3 M^{-1} cm^{-1}) of 15.4 (A), 11.7 (G), 7.3 (C), and 8.8 (U). For radiolabeling, 25−50 pmol of RNA was dephosphorylated (if required) with calf intestinal phosphatase (CIP, Boehringer), then incubated with 25 pmol γ-[^{32}P]ATP (6000 Ci/mmol, NEN) and 10 units of T4 polynucleotide kinase (PNK, NEB) for 10−30 min, followed by PAGE and isolation as above.

RNAs Prepared by Splint Ligations. All P4−P6 RNAs incorporating 2′-deoxy or 2′-methoxy substitutions were prepared by ligation reactions mediated by DNA splints (*15*, *16*). The RNAs were constructed stepwise from combinations of in vitro T7 transcripts and synthetic RNA oligoribonucleotides, using DNA oligonucleotides as splints, as summarized in Figure 2. RNA oligos were purchased from Dharmacon Research (Boulder, CO) or prepared by standard solid-phase methods on an Applied Biosystems synthesizer; all were purified by 20% PAGE. Plasmid DNAs encoding T7 transcripts **A**−**E** were prepared by PCR from the wild-type P4−P6 plasmid. All constructs were subcloned into pUC19 and verified by automated sequencing over both ligation sites. DNA templates for transcripts **A**, **C**, and **E** retained the *Ear*I linearization site of wild-type P4−P6 such that the transcripts

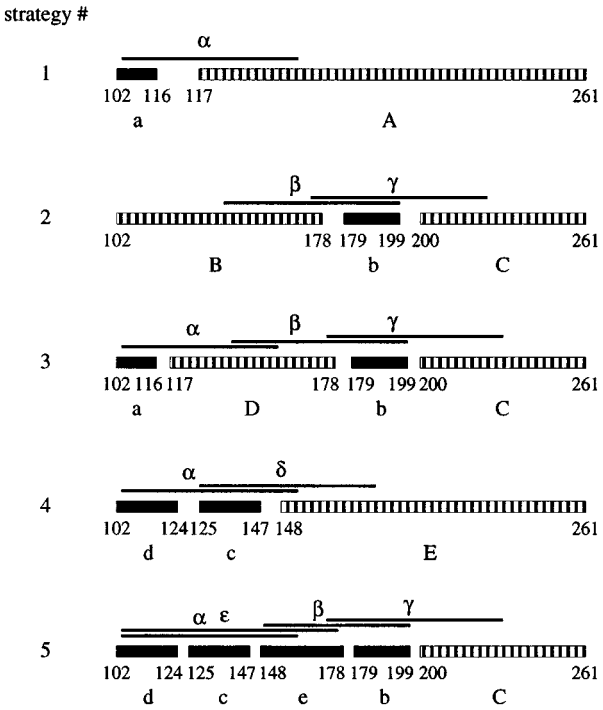

FIGURE 2: Ligation strategies to prepare P4−P6 derivatives with 2′-substitutions. The RNA building blocks are denoted by boldface capital letters (T7 transcripts **A**−**E**, shown as striped bars) or boldface lowercase letters (synthetic RNA oligoribonucleotides **a**−**e**, shown as solid bars); DNA splints are denoted by Greek letters (α−ϵ, shown as solid lines). The wild-type P4−P6 sequence comprises two artificial guanosine nucleotides at its 5′ end (for in vitro T7 transcription) plus nucleotides 104−261 of the *Tetrahymena* group I intron, for a total of 160 nucleotides. For convenience, the initial two Gs are referred to as nucleotides 102−103. DNA splints were as follows (5′ to 3′ direction): α, nt 154−104; β, nt 199−149; γ, nt 225−175; δ, nt 174−125; ϵ, nt 175−104. In strategy 5, splint ϵ (72 nt) is longer than the other splints (50−51 nt) so that it does not comigrate on PAGE with the 54 nt product **c**−**e**. The transcripts and oligos are shown to scale, but the splints are slightly off-scale because of gaps between the transcripts and/or oligos. In several cases not described, three-way ligations (three RNA oligos and/or T7 transcripts with one or two DNA splints) were attempted, but yields were extremely poor.

end at P4−P6 nucleotide 261, as does wild-type P4−P6. DNA templates for transcripts **B** and **D** were designed with 3′-hammerhead ribozymes as described (*13*) such that in situ hammerhead processing of the initial transcript provides RNA truncated at P4−P6 nucleotide 178. The resulting processed transcript has a 2′,3′-cyclic phosphate at the 3′ end, which was removed with PNK before ligation as described below. Plasmids were linearized with *Ear*I (**A**, **C**, **E**) or *Hin*dIII (**B**, **D**). T7 RNA polymerase reaction conditions for transcripts **A**−**E** were as follows. **A** and **D**, 20 μg/mL linearized plasmid DNA, 40 mM Tris, pH 8.0, 10 mM DTT, 10 mM $MgCl_2$, 1 mM each NTP, 2 mM spermidine, 10 mM GMP, 37 °C, 5 h (**A**) or 9 h (**D**), purified by 6% PAGE (**A**) or 8% PAGE (**D**). **B**, 20 μg/mL linearized plasmid DNA, 40 mM Tris, pH 8.0, 20 mM DTT, 30 mM $MgCl_2$, 4 mM each NTP, 2 mM spermidine, 37 °C, 9 h, purified by 8% PAGE. **C** and **E**, 20 μg/mL linearized plasmid DNA, 40 mM Tris, pH 8.0, 20 mM DTT, 10 mM $MgCl_2$, 1 mM each NTP, 2 mM spermidine, 10 mM GMP, 37 °C (**C**) or 25 °C (**E**), 21 h, purified by 8% PAGE. Note that because transcripts **A** and **C**−**E** were subsequently used as 3′ partners in ligation reactions, which require a 5′-monophosphate, 10 mM GMP was included in the transcriptions to incorporate a 5′-monophosphate in the majority of the transcripts. Control RNAs C1−C5 with the wild-type P4−P6 sequence (no 2′-substitutions) were prepared by ligation using strategies 1−5 of Figure 2, respectively.

In a typical ligation reaction, the desired amounts of oligos and/or transcripts and DNA splint (see specifics below) were combined and precipitated with 0.1 vol of 3 M NaCl and 3 vol of ethanol at −20 °C for several hours and isolated by centrifugation. If required by the ligation strategy, the RNA partners were first reacted with T4 polynucleotide kinase (PNK, New England Biolabs) to phosphorylate the 5′-end (typically ∼5 nmol of RNA oligo with 50 units of PNK, 100 μL, 37 °C, 1 h) or to hydrolyze and remove a 2′,3′-cyclic phosphate from the 3′-end (typically ∼5 nmol of RNA transcript with 125 units of PNK in 0.1 M sodium phosphate, pH 6.0, no ATP, 5 mM DTT, 200 μL, 37 °C, 18 h). Note that PNK sold by Boehringer has a mutation that removes 3′-phosphatase activity; this particular enzyme is *inactive* for hydrolysis and removal of the 2′,3′-cyclic phosphate group. The pellet was redissolved in 0.8 vol of buffer TE (10 mM Tris, pH 8.0, and 1 mM EDTA), e.g., 200 μL of TE for a final ligation reaction volume of 250 μL. The sample was annealed by heating to 90 °C for 3 min in a heat block, allowed to cool slowly to room temperature (60−90 min), and placed on ice. After several minutes, 0.1 vol of 10× ligase buffer (500 mM Tris, pH 8.0, 100 mM $MgCl_2$, 100 mM DTT, 10 mM ATP, and 0.5% Triton X-100) and then 0.1 vol of T4 DNA ligase (Pharmacia, FPLCpure, cat. no. 27-0870-04, ∼6000 Weiss units/mL) were added, and the reaction tube was mixed and placed at 37 °C for 4 h. The reaction was quenched with 2 vol of stop solution (80% formamide, 1× TBE, 50 mM EDTA, 0.025% each bromphenol blue and xylene cyanol), and ligation products were separated by PAGE. Ligation reactions and yields for strategies 1−5 of Figure 2 are summarized in Table 1. Occasionally, yields were lower than the ranges reported, but this was not reproducible as repeating the reactions almost always gave yields within the stated range. In the last steps of strategies 2 and 3 and in one case for strategy 1, a side product was sometimes observed migrating slightly faster than the desired 160 nucleotide P4−P6 derivative (this side product was not characterized further). We are unable to explain this observed variability—certain ligation reactions appear to be highly sensitive to precise reaction conditions.

Nondenaturing (Native) Gel Electrophoresis. Gels (26 cm width x 17 cm height x 0.5 mm thickness) were prepared with 1× TB buffer without EDTA (89 mM Tris and 89 mM boric acid, pH ∼8.5) and 8% acrylamide:bisacrylamide (29:1, Fisher 40% stock), polymerized by addition of 1/100 by volume of 10% ammonium persulfate and 1/1000 by volume of TEMED. $MgCl_2$ was added to the desired concentration before polymerization. Running buffer was 1× TB with $MgCl_2$ at the desired concentration. Samples were prepared from 2 μL of radiolabeled stock solution in water plus 2 μL of 2× loading buffer (2× buffer is 2× TB, 10% glycerol, and twice the final desired $MgCl_2$ concentration). Samples were heated at 50 °C for 5 min, then cooled at 35 °C for 5−10 min before loading. Gels were run at 35 °C, 150−200 V for 4−6 h, dried, and exposed to a PhosphorImager screen. Images were scanned and analyzed with ImageQuant 4.0 (Molecular Dynamics).

Table 1: Splint Ligation Synthesis of P4−P6 Derivatives[a]

step	nmol	RNA 1	nmol	RNA 2	nmol	splint	product	nt	μL rxn	% gel	% yield[b]
Strategy 1 (for Substitutions at C109 and/or G110 Only)											
1	2.5	**a**	3.0	**A**	2.5	α	**a-A**	160	200	12	35−40
Strategy 2 (for Substitutions at A183, A184, and/or A186 Only)											
1	5.5	**B**[c]	5.0	**b**[d]	5.0	*β*	**B-b**	98	250	6	23−37
2	0.50	**B-b**	0.55	**C**	0.50	*γ*	**B-b-C**	160	90	6	26−32
Strategy 3 (for Substitutions at C109/G110 and Also A183/A184)											
1	10	**a**	11−12	**D**	10	α	**a-D**	77	250	8	35−68
2	5.5	**a-D**[c]	5.0	**b**[d]	5.0	*β*	**a-D-b**	98	250	6	12−38
3	0.50	**a-D-b**	0.55	**C**	0.5	*γ*	**a-D-b-C**	160	90	6	26−32
Strategy 4 (for Substitution at C137 Only)											
1	4.8	**c**[d]	4.0	**E**	4.0	*δ*	**c-E**	137	250	6	37−42
2	1.68	**d**	1.40	**c-E**	1.40	α	**d-c-E**	160	90	6	11−14
Strategy 5 (for Substitution at C137 and A186)											
1	5.0	**b**[d]	5.5	**C**	5.0	*γ*	**b-C**	83	250	8	26−29
2	10	**c**[d]	10	**e**	10	*ϵ*	**c-e**	54	250	10	56−67
3	5.0	**d**	5.0	**c-e**	5.0	α	**d-c-e**	77	250	8	11−14
4	0.50	**d-c-e**	0.50	**b-C**	0.50	*β*	**d-c-e-b-C**	160	90	6	27

[a] See text for experimental details of construction of the P4−P6 derivatives of Figure 2 by splint ligation. T7 transcripts are shown as boldface uppercase letters; synthetic RNA oligonucleotides as boldface lowercase letters; and DNA splints as Greek letters. [b] All yields are reported for the single ligation step indicated. [c] 2′,3′-Cyclic phosphate hydrolyzed and removed with PNK. [d] 5′-Phosphorylated with PNK.

Four rounds of native gels were performed on wild-type P4−P6, P4−P6-bp, and the various 2′-deoxy and 2′-methoxy derivatives described in the text (Figure 3). Multiple (3−4) samples of wild-type P4−P6 and P4−P6-bp were spaced approximately evenly across each gel to provide an experimental baseline for the mobility measurements. Deviations from perfectly horizontal were small (<1% for all gels). Gel images were transferred to Adobe Illustrator 6.0, and lines were drawn through the centers of the 3−4 bands for the unfolded control P4−P6-bp and across the loading baseline (enough PhosphorImager counts were present in the wells to allow this). For every P4−P6 sample, the relative mobility was determined by taking the ratio of the vertical distances from the baseline to the test sample and from the baseline to the P4−P6 bp line. These relative mobility values were used to obtain thermodynamic parameters as described in the next subsection. For each round, gels were run at the following Mg^{2+} concentrations (mM): 0.1, 0.2, 0.33, 0.5, 0.6, 0.7, 0.85, 1.0, 1.2, 1.5, 2.2, 3, 4, 5, 10, 20, and 30. For gels at ≤10 mM Mg^{2+}, the pH difference between the upper and lower buffers at the end of the run was <0.4 pH units and typically <0.2 pH units at the lower Mg^{2+} concentrations. For gels at 20 mM Mg^{2+}, the pH difference was ∼1 pH unit, while for gels at 30 mM Mg^{2+}, the pH difference was ∼1.5 pH units. For the third round of gels, additional gels were run at 20 and 30 mM Mg^{2+} with hourly buffer changes so that the observed pH difference did not exceed 0.4 pH units. The relative mobilities of the P4−P6 derivatives tested in this way were approximately unchanged relative to gels run without frequent buffer changes (data not shown). This shows that pH differences during the runs did not distort our results, and in any case, only data from 0.1 to 10 mM Mg^{2+} were used to extract thermodynamic parameters presented in the text.

Because our standard 1× TB buffer contains no monovalent ions (Na^+ or K^+) and because monovalents can be involved in RNA structure (*17*), we tested whether exclusion of monovalent ions affects our results. For the second round of gels, additional gels were run with running buffers that included 1.5 mM Mg^{2+}/30 mM Na^+; 1.5 mM Mg^{2+}/30 mM K^+; or 5 mM Mg^{2+}/30 mM K^+. In all cases, the rank mobility order for the tested P4−P6 derivatives was unaltered. Moreover, the values of relative mobilities were approximately unchanged; there was perhaps a slight *retardation* of mobility upon inclusion of monovalents (see Supporting Information). This effect is in the direction opposite to that expected if monovalents were required for proper structure, so we conclude that exclusion of monovalents is unimportant in our assay.

Thermodynamic Analysis. The wild-type P4−P6 RNA sequence has an apparent standard free-energy change $\Delta G^{\circ\prime}$(wt) associated with its tertiary folding triggered by Mg^{2+}. The equilibrium of interest is

$$\mathrm{U} + n\mathrm{Mg}^{2+} \rightleftharpoons \mathrm{F}\cdot n\mathrm{Mg}^{2+} \quad (1)$$

where U is unfolded P4−P6 (intact secondary structure but no long-range tertiary structure) and $F\cdot nMg^{2+}$ is folded P4−P6. This model assumes that n Mg^{2+} ions are specifically bound in the folded state, but it does not prohibit more loosely associated Mg^{2+} ions from nonspecifically stabilizing the folded state. The folding free energy is related to the Mg^{2+} concentration required for folding according to the following simple derivation. In general,

$$\Delta G' = \Delta G^{\circ\prime} + RT \ln([\mathrm{F}\cdot n\mathrm{Mg}^{2+}]/[\mathrm{U}][\mathrm{Mg}^{2+}]^n) \quad (2)$$

At equilibrium, $\Delta G' = 0$, and at the midpoint of the folding transition where half the molecules are folded, [U] = $[F\cdot nMg^{2+}]$. Therefore, from eq 2

$$\Delta G^{\circ\prime} = +nRT \ln[\mathrm{Mg}^{2+}]_{1/2} \quad (3)$$

where $[Mg^{2+}]_{1/2}$ is the concentration of Mg^{2+} necessary for folding of half of the molecules. Note the sign of nRT is positive because the n Mg^{2+} ions appear on the *left* side of eq 1. Values for $[Mg^{2+}]_{1/2}$ were obtained by fitting (KaleidaGraph v3.0.2) the experimental relative mobility versus $[Mg^{2+}]$ data such as that shown in Figure 4 from 0.1 to 10 mM Mg^{2+} to the four-parameter standard titration equation:

$$M_{\mathrm{obs}} = (M_{\mathrm{low}} + M_{\mathrm{high}}\cdot K\cdot[\mathrm{Mg}^{2+}]^n)/(1 + K[\mathrm{Mg}^{2+}]^n) \quad (4)$$

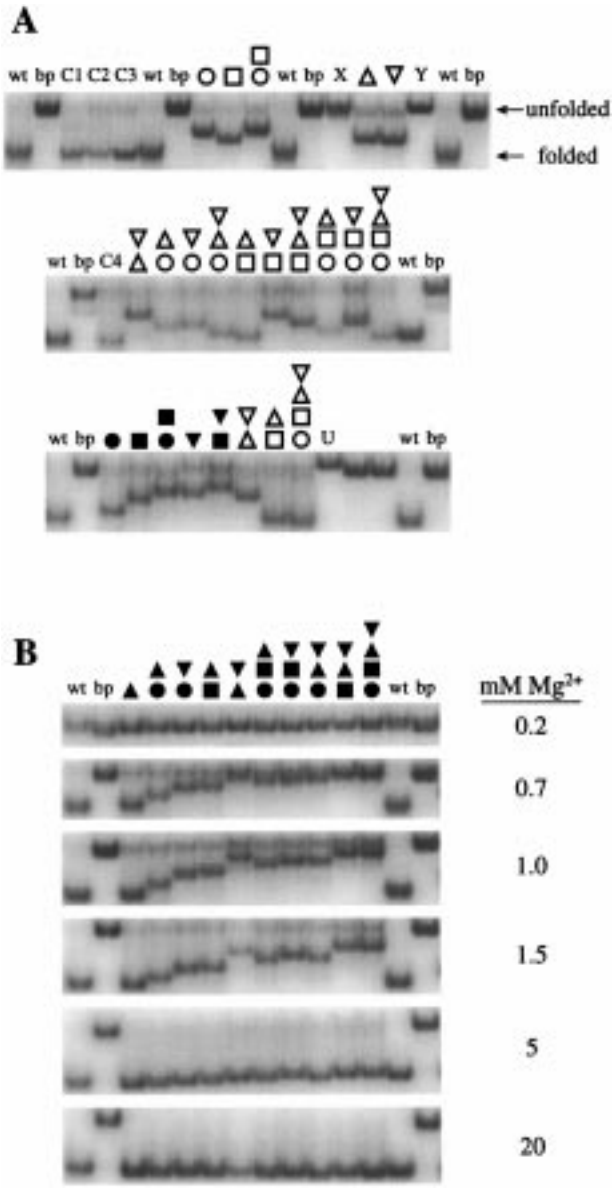

FIGURE 3: Representative nondenaturing gels of P4−P6 derivatives. (A) Mg^{2+} gels (1.0 mM) from rounds 1−3. The "folded" arrow shows the migration of wild-type P4−P6; the "unfolded" arrow indicates the migration of unfolded control P4−P6-bp. (B) Gels from Round 4 at various Mg^{2+} concentrations. Lanes are labeled to indicate the P4−P6 derivative as follows: wt, wild-type P4−P6; bp, P4−P6 J5/5a-base-paired (P4−P6-bp) unfolded control; circle, C109 substitution; square, G110 substitution; triangle, A183 substitution; inverted triangle, A184 substitution (filled symbols are 2′-deoxy derivatives; open symbols are 2′-methoxy derivatives); X, C137-2′-methoxy derivative; Y, A186-2′-methoxy derivative; C1−C4 are wild-type controls prepared by splint ligation as described in the Materials and Methods. In the round 3 gel, we also ran P4−P6 A186U (lane labeled U). The two lanes to the right of A186U are the previously described J5/5a mutants P4−P6−U1 and P4−P6−U1+U2, which destabilize tertiary folding (*21*). In most cases, P4−P6 derivatives prepared by ligation showed a relatively faint band comigrating with P4−P6-bp at all Mg^{2+} concentrations. Because similar such bands were seen for the wild-type control RNAs C1−C5 as for P4−P6 derivatives with 2′-substitutions, we assume these bands represent a minor amount of degradation occurring in at least one ligation step or associated gel purification. In any case, these faint bands appear not to distort our results, since the $[Mg^{2+}]_{1/2}$ values for the wild-type controls C1−C5 were unchanged relative to transcribed wild-type P4−P6.

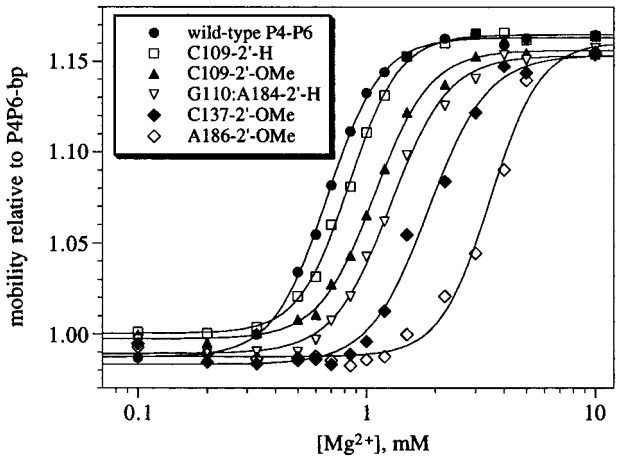

FIGURE 4: Mg^{2+} titration curves for folding of wild-type P4−P6 and representative 2′-deoxy and 2′-methoxy derivatives at 35 °C. The mobilities of each P4−P6 RNA on nondenaturing gels including those of Figure 3 were measured relative to the unfolded control P4−P6-bp and fit to a standard titration curve as described in the Materials and Methods. From left to right, the fit values of $[Mg^{2+}]_{1/2}$ are 0.67, 0.84, 1.08, 1.27, 1.86, and 3.47 mM; the fit values of the Mg^{2+} Hill coefficient n are 3.7, 4.0, 3.6, 3.4, 3.4, and 4.0. The calculated values of $\Delta\Delta G^{\circ\prime}$ are tabulated in Table 2 for these and all the other 2′-deoxy and 2′-methoxy derivatives. The average value of $[Mg^{2+}]_{1/2}$ for wild-type P4−P6 over the four rounds of gels (13 determinations) was 0.67 ± 0.03 mM.

where M_{obs} is the observed relative mobility as a function of $[Mg^{2+}]$, M_{low} and M_{high} are the limiting low and high values of relative mobility at low and high $[Mg^{2+}]$, and K and n are the equilibrium constant and Mg^{2+} Hill coefficient for eq 1. $[Mg^{2+}]_{1/2}$ values were calculated from the fit values of K and n as $K^{-1/n}$. For any given P4−P6 mutant, we define the change in tertiary folding $\Delta\Delta G^{\circ\prime}$ by eq 5.

$$\Delta\Delta G^{\circ\prime} = \Delta G^{\circ\prime}(\text{mutant}) - \Delta G^{\circ\prime}(\text{wt}) \qquad (5)$$

We may then estimate $\Delta\Delta G^{\circ\prime}$ for any particular mutant according to $\Delta\Delta G^{\circ\prime} = nRT \ln([Mg^{2+}]_{1/2,mut}/[Mg^{2+}]_{1/2,wt})$. In practice, for each round of gels, we instead computed the $\Delta G^{\circ\prime}$ for each mutant and for wild-type P4−P6 according to eq 3, using the $[Mg^{2+}]_{1/2}$ values from the data fitting and $n = 4$ as described below. We averaged the three to four determinations of $\Delta G^{\circ\prime}$(wt) from each gel. For each mutant, we then took the difference in $\Delta G^{\circ\prime}$s to obtain $\Delta\Delta G^{\circ\prime}$ according to eq 5.

The curve fits provide best values and error estimates (σ) for K and n for each P4−P6 derivative. The error on any single determination of $\Delta\Delta G^{\circ\prime}$ was rarely greater than ±0.2 kcal/mol for any combination of 2′-substitutions at C109/G110/A183/A184; note that this error has contributions from $\Delta G^{\circ\prime}$ for both the mutant of interest and for wild-type P4−P6 determined on the same set of gels. The error of ±0.2 kcal/mol is similar to that observed in multiple determinations of $\Delta\Delta G^{\circ\prime}$ for the same mutant (see Supporting Information).

In the four rounds of gels, the experimental values ($\pm\sigma$) of the Mg^{2+} Hill coefficient n for wild-type P4−P6 were 4.26 ± 0.11, 3.73 ± 0.25, 4.07 ± 0.03, and 3.69 ± 0.07; the weighted average (weights = $1/\sigma^2$) of these values is approximately 4 (4.02 ± 0.03). Furthermore, for all P4−P6 derivatives with 2′-deoxy or 2′-methoxy substitutions at positions C109, G110, A183, and/or A184, the experimental value of n was not much different than 4 (see Supporting

Table 2: Destabilization of P4−P6 RNA Tertiary Folding at 35 °C by 2′-Deoxy and 2′-Methoxy Substitutions[a]

	2′-deoxy		2′-methoxy	
site(s) substituted	$\Delta\Delta G^{\circ\prime}$ (kcal/mol)	no. of deleted H-bonds	$\Delta\Delta G^{\circ\prime}$ (kcal/mol)	no. of deleted H-bonds
C109	0.4 (2)	1	1.1 (2)	1
G110	1.0 (2)	2	0.8 (2)	1
A183	0.2	1	0.8	1
A184	1.1	2	0.8	1
C109:G110	1.4 (2)	3	1.2 (2)	2
C109:A183	0.7	2	0.7	2
C109:A184	1.2	2	0.8	2
G110:A183	1.3	2	0.1 (2)	2
G110:A184	1.6 (2)	4	1.2	2
A183:A184	2.0	3	1.2 (2)	2
C109:G110:A183	1.7	3	0.3 (2)	3
C109:G110:A184	1.8	4	0.8	3
C109:A183:A184	1.8	3	0.3	3
G110:A183:A184	2.2	4	0.8	3
C109:G110:A183:A184	2.3	4	−0.2 (2)	4
C137	nd	1	2.5 (3)	1
A186	nd	2	4.1 (3)	1

[a] $\Delta\Delta G^{\circ\prime}$ values were calculated from the nondenaturing gel Mg^{2+} titration curves (Figure 4) as $\Delta G^{\circ\prime}$(mutant) − $\Delta G^{\circ\prime}$(wt) as described in the Materials and Methods. Positive values for $\Delta\Delta G^{\circ\prime}$ indicate that a higher $[Mg^{2+}]$ is required to fold the P4−P6 derivative and thus indicate destabilization of the folded P4−P6 molecule. The number of hydrogen bonds deleted in each derivative is tabulated (see Figure 1). For each derivative, the number of $\Delta\Delta G^{\circ\prime}$ determinations is shown in parentheses; when no number is shown, only a single determination was performed. Both from the error in each single determination and from the derivatives for which more than one determination was performed, we estimate the error in reported $\Delta\Delta G^{\circ\prime}$ values as ±0.2 kcal/mol or less when $\Delta\Delta G^{\circ\prime} < 2.4$ kcal/mol. For example, our *worst* case is the G110:A184 2′-deoxy mutant, for which two determinations of $\Delta\Delta G^{\circ\prime}$ gave values of 1.4 and 1.7 kcal/mol. A complete tabulation of $\Delta\Delta G^{\circ\prime}$s and error estimates is provided in the Supporting Information. nd, not determined.

Information). Because these sites of substitution were chosen specifically to disrupt individual hydrogen bonds without disrupting global structure, and because the mutants' experimental Hill coefficients were very similar to that of wild-type P4−P6, we consider it highly unlikely that the "true" value of n is altered in any of these derivatives. Therefore, we take $n = 4$ to compute $\Delta G^{\circ\prime}$ values according to eq 3. If the true value of n differs from the experimental value of 4, then the $\Delta\Delta G^{\circ\prime}$ values computed with eq 5 would scale accordingly, but the rank order of $\Delta\Delta G^{\circ\prime}$ values for the various P4−P6 derivatives would remain unchanged.

A criterion for an equilibrium measurement is that the final folded state of the molecule should not depend on the direction from which the folding equilibrium is approached. To test this directly, we prepared two samples each of wild-type P4−P6, P4−P6-bp, and several representative P4−P6 derivatives from Table 2. One sample of each pair was annealed at 10 mM Mg^{2+}, where the RNA is fully folded; the second sample was annealed at a lower Mg^{2+} concentration present in the gel and buffer. We then electrophoresed each pair of samples in adjacent lanes on native gels prepared with 0.1, 0.5, 1.0, or 5 mM Mg^{2+} in the gel and buffer as usual. In all cases, the concentration of Mg^{2+} in the annealing step had no effect on the relative P4−P6 mobility (data not shown), demonstrating that the path of approach to folding equilibrium does not affect the final folded state for the molecules examined.

Temperature Gradient Gel Electrophoresis (TGGE). TGGE experiments were performed essentially as described (*18*), with several modifications. To facilitate comparison between the TGGE and Mg^{2+}-dependent native gel results, we used 1× TB (Tris-borate) as the TGGE running buffer, instead of a Tris-Hepes-Na^+ buffer as in the previous report (*18*). Note that $[Mg^{2+}]_{1/2}$ for wild-type P4−P6 is 0.67 mM in 1× TB but ∼0.9 mM in the Tris-Hepes-Na^+ buffer. The temperature gradient within the gel was between approximately 15 and 56 °C. A modified form of the "R_f method" (*18*) was used to extract thermodynamic information from the gels in two steps. First, the raw mobility data (calculated at 40 evenly spaced temperature points across each gel) were plotted versus temperature and fit to the three-parameter rearranged van't Hoff equation $M_{obs} = [e^X \cdot (M_{max} - 1)/(1 + e^X)] + 1$, where M_{obs} is the observed relative mobility at temperature T, $X \equiv -\Delta H^{\circ\prime}/RT + \Delta S^{\circ\prime}/R$, and M_{max} is the maximum relative mobility. This provided a fit value of the maximum relative mobility M_{max} and an associated error estimate ($\pm\sigma$); the $\Delta H^{\circ\prime}$ and $\Delta S^{\circ\prime}$ from this fit had substantial error (typically ±5−6 kcal for $\Delta H^{\circ\prime}$) and were not used further. Such an objective method is preferable to subjective visual identification of M_{max}, because its value strongly affects the final results as described shortly. Second, the fit value of M_{max} was used to calculate the equilibrium constant K_{eq} from each of the 40 data points, using the best estimate of M_{max} and also using the best estimate $\pm\sigma$ (three K_{eq} values for each temperature point). Finally, three van't Hoff plots of ln K_{eq} versus reciprocal temperature (as in Figure 6) were used to obtain values for the thermodynamic parameters $\Delta H^{\circ\prime}$ and $\Delta S^{\circ\prime}$ over the range of maximum relative mobilities. The resulting ranges of $\Delta H^{\circ\prime}$ and $\Delta S^{\circ\prime}$ were severalfold larger than the statistical error from fitting each individual van't Hoff plot, indicating that a substantial part of the error in $\Delta H^{\circ\prime}$ and $\Delta S^{\circ\prime}$ arises from the error in determining M_{max} instead of in fitting the van't Hoff plots. Therefore, the calculated ranges of $\Delta H^{\circ\prime}$ and $\Delta S^{\circ\prime}$ were converted to values of average ± (half of range) as the best values for $\Delta H^{\circ\prime}$ and $\Delta S^{\circ\prime}$ ($\pm\sigma$). Weighted averages (weights $= 1/\sigma^2$) of three such determinations of $\Delta H^{\circ\prime}$ and $\Delta S^{\circ\prime}$ for each P4−P6 RNA are reported in the text.

Three-Piece Catalytic Activity Kinetic Assay. The abilities of substituted P4−P6 RNAs to reconstitute ribozyme activity were evaluated using the previously reported kinetic assay (*19*). The P1−P3 RNA, P3−P9 RNA, and buffer composition (including 5 mM spermidine) were as previously reported (*19*). Reactions (50 μL) were preincubated at 50

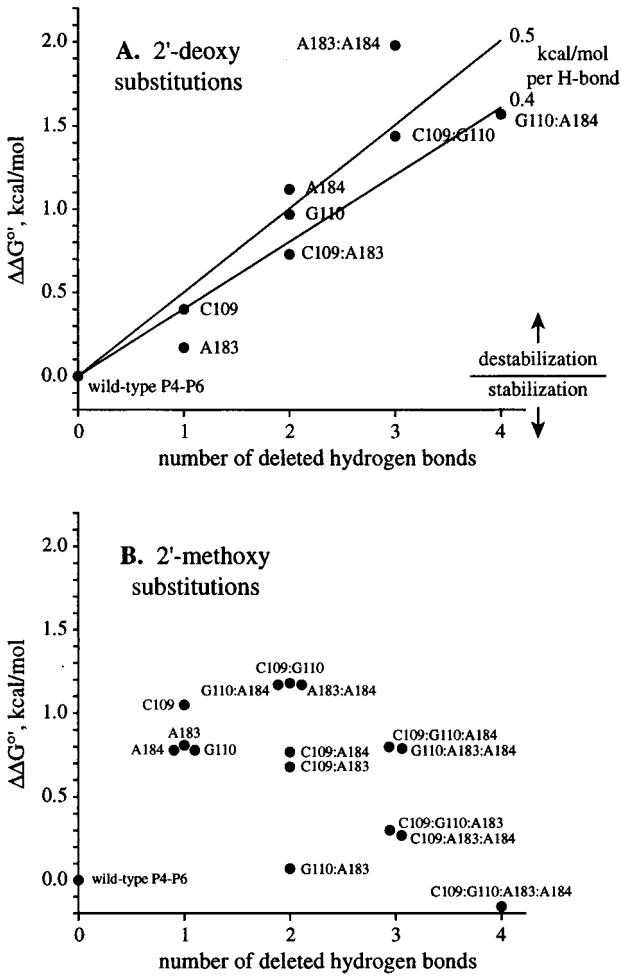

FIGURE 5: Dependence of tertiary folding $\Delta G^{\circ\prime}$ on substitution of 2′-hydroxyl groups at P4−P6 nucleotides C109, G110, A183, and A184. (A) 2′-Deoxy substitutions. The change in folding $\Delta G^{\circ\prime}$ [$\Delta\Delta G^{\circ\prime} = \Delta G^{\circ\prime}$(mutant) − $\Delta G^{\circ\prime}$(wt)] at 35 °C is plotted versus the number of deleted hydrogen bonds for all nonredundant 2′-deoxy derivatives of Table 2. As described in the text, a 2′-deoxy derivative is redundant if it comprises two or more 2′-deoxy substitutions which disrupt the same hydrogen bond (e.g., C109 and A184; see Figure 1). (B) Same analysis for all 2′-methoxy substitutions, of which none are redundant.

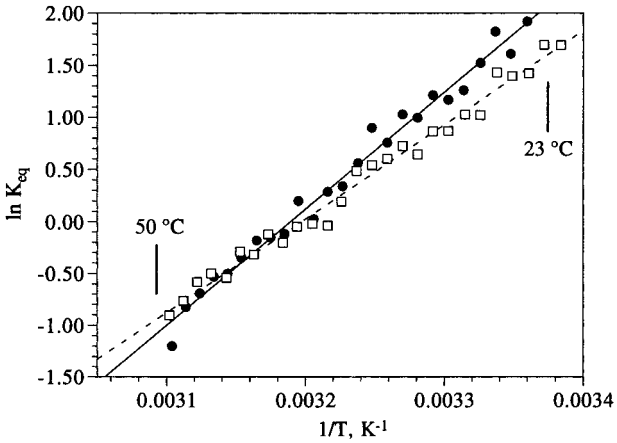

FIGURE 6: Representative van't Hoff plots from temperature gradient gel electrophoresis (TGGE) experiments. Filled circles and solid line, wild-type P4−P6; open squares and dashed line, quadruple 2′-methoxy derivative C109:G110:A183:A184. The best fit values for these individual experiments are wild-type, $\Delta H^{\circ\prime} = -22.2 \pm 0.6$ kcal/mol and $\Delta S^{\circ\prime} = -70.9 \pm 1.9$ eu; quadruple 2′-methoxy derivative, $\Delta H^{\circ\prime} = -17.9 \pm 0.4$ kcal/mol and $\Delta S^{\circ\prime} = -57.3 \pm 1.4$ eu. The overall best fit values for three combined runs of each P4−P6 RNA are given in the text.

°C for 10 min, then at 25 °C for 5 min, and finally initiated at 25 °C with prewarmed $MgCl_2$ to 50 mM and GTP to 5 mM. Under these conditions and with 1 nM radiolabeled P1−P3, 100 nM P3−P9, and 100 nM P4−P6, in our hands the half-life, $t_{1/2}$, for wild-type P4−P6 was ∼7 min (∼5 min at 80 mM Mg^{2+} and 25 °C). We have no immediate explanation for why our absolute rate is faster than that previously reported (wild-type $t_{1/2}$ reported on the order of 35 min at 80 mM Mg^{2+} and 40 °C). The $t_{1/2}$ for P4−P6-bp at 50 mM Mg^{2+} and 25 °C was ∼124 min. In addition to a zero timepoint, reaction aliquots were quenched at 0, 1, 2, 3.5, 5, 10, 20, 60, and 120 min after initiation and electrophoresed on 20% denaturing polyacrylamide gels. Catalytic rates were obtained by fitting a straight line with slope $-k_{obs}$ to the initial (4−6) points of a plot of ln(fraction substrate) versus time.

RESULTS

Mg^{2+} Dependence of P4−P6 Folding Can Be Quantitated on Nondenaturing Gels. The major Mg^{2+}-dependent tertiary folding transition in P4−P6 juxtaposes the P5abc and P4+P6 subdomains of the RNA (*14*). In addition to a significant number of Mg^{2+} interactions that stabilize the resulting folded state (*20*), several long-range intramolecular hydrogen bonds are observed in the X-ray crystal structure (*3*). Four of these hydrogen bonds are in the C109/A184 and A183/G110 ribose zipper motif (Figure 1). The tertiary folding transition also changes the nondenaturing gel mobility of P4−P6 (*21, 22*), and here we take advantage of this change to monitor P4−P6 folding and extract thermodynamic information. Without Mg^{2+}, P4−P6 has secondary structure, but its tertiary structure is unfolded; its extended conformation causes it to migrate relatively slowly through the gel matrix. Adding millimolar Mg^{2+} allows tertiary interactions to form, and the molecule folds upon itself into a more compact conformation that migrates more rapidly (Figure 3).

At an intermediate Mg^{2+} concentration or upon destabilization of tertiary folding by mutation, the RNA is in rapid equilibrium between two states: unfolded (secondary structure only) and folded (secondary and tertiary structure). Under these conditions, the RNA has an intermediate electrophoretic mobility, which may be quantified as a function of the Mg^{2+} concentration (*21*). Previous work has shown that the Mg^{2+}-dependent folding of an RNA containing P4−P6 does not depend on the direction from which the folding equilibrium is approached (*23*), and we demonstrated this directly for folding of P4−P6 and several representative derivatives (see Materials and Methods). We performed multiple gel experiments over a range of $[Mg^{2+}]$ from 0.1 to 10 mM, comparing the mobility of wild-type P4−P6 to the unfolded control P4−P6 J5/5a-base-paired (P4−P6-bp), which is locked into the extended conformation (*14*). The relative mobility of P4−P6 was plotted versus $[Mg^{2+}]$ and fit to a standard titration curve (Figure 4). Wild-type P4−P6 has a folding midpoint at $[Mg^{2+}]_{1/2} = 0.67$ mM at 35 °C, and the experimental Mg^{2+} Hill coefficient is approximately 4.

Substitutions at 2′-Hydroxyls Increase the Mg^{2+} Requirement for P4−P6 Folding. We systematically substituted P4−

P6 nucleotides C109, G110, A183, and A184 in all combinations with their 2′-deoxy or 2′-methoxy analogues, a total of 30 mutants altogether (the 2′-deoxy and 2′-methoxy substitutions were never mixed in the same P4−P6 derivative). All the derivatives were prepared by splint ligation (*15*, *16*). Each derivative displayed a Mg^{2+}-dependent folding transition on nondenaturing gels that was qualitatively similar to that of wild-type P4−P6 (Figure 3). Only the particular Mg^{2+} concentration required for folding was changed. We measured the mobility of each P4−P6 derivative relative to the unfolded control P4−P6-bp at [Mg^{2+}] from 0.1 to 10 mM and determined the $[Mg^{2+}]_{1/2}$ as for wild-type (Figure 4). In all cases, the experimental Hill coefficient was within 0.5 of that for wild-type P4−P6 assayed in parallel on the same set of gels, as detailed in the Supporting Information. The change in tertiary folding free energy for each derivative relative to wild-type P4−P6 ($\Delta\Delta G^{\circ\prime}$) was calculated as described in the Materials and Methods. Above 10 mM Mg^{2+}, there was a slight increase in relative mobility (data not shown) that is not an artifact of pH changes during the run (see Materials and Methods). We have not examined this effect further, but it may reflect a real structural transition in P4−P6 at very high [Mg^{2+}]. In any case, relative mobility data at ≥20 mM Mg^{2+} were not used to fit the folding transition monitored from 0.1 to 10 mM Mg^{2+}.

2′-Deoxy Substitutions Indicate ~1.0 kcal/mol per "Tooth" of the Ribose Zipper Examined. A 2′-deoxy substitution may disrupt either one or two hydrogen bonds of a ribose zipper motif, depending on which hydrogen-bonding partner is affected. If partner II is mutated, two hydrogen bonds are deleted by a single deoxy substitution, while if partner I is mutated, only one hydrogen bond is deleted (Figure 1). Table 2 summarizes the $\Delta\Delta G^{\circ\prime}$ values for the complete set of 2′-deoxy derivatives over the four P4−P6 positions examined. Both hydrogen bonds of the C109/A184 interaction should be eliminated in the A184 single mutant (observed $\Delta\Delta G^{\circ\prime} = 1.0$ kcal/mol) and also in the C109:A184 double mutant (1.2 kcal/mol). Similarly, both hydrogen bonds of the A183/G110 interaction should be eliminated in the G110 single mutant (observed $\Delta\Delta G^{\circ\prime} = 1.0$ kcal/mol) and in the G110:A183 double mutant (1.3 kcal/mol). Thus, our data give a consistent value of ~−1.0 kcal/mol per tooth of the ribose zipper motif, where each tooth comprises *two* hydrogen bonds. The slightly higher values in the double mutants may reflect additional destabilization inherent to the 2′-deoxy substitution, as described below. On the other hand, the C109 and A183 single mutants destabilize P4−P6 folding only slightly ($\Delta\Delta G^{\circ\prime} = 0.4$ and 0.2 kcal/mol, respectively). Therefore, partner II of a ribose zipper tooth is essential for structural stability, whereas partner I has more of a supporting role, just as one might predict from Figure 1.

Individual Ribose Zipper Hydrogen Bonds Contribute −0.4 to −0.5 kcal/mol to RNA Folding. Another way to analyze the 2′-deoxy data is to plot the change in folding free energy $\Delta\Delta G^{\circ\prime}$ versus number of deleted hydrogen bonds (Figure 5A; the subset of mutations plotted is described below). We also include a point for zero mutations (i.e., wild-type P4−P6), defined to have $\Delta\Delta G^{\circ\prime} = 0$. The data are best described by a relatively consistent $\Delta\Delta G^{\circ\prime}$ of 0.4−0.5 kcal/mol per hydrogen bond deleted; that is, each hydrogen bond of the particular ribose zipper we studied contributes −0.4 to −0.5 kcal/mol to the tertiary folding $\Delta G^{\circ\prime}$.

Correction for Side Effects of 2′-Deoxy Substitution. One particular concern with mutating 2′-hydroxyls to study hydrogen bond deletions is that the substitutions may have side effects other than hydrogen bond disruption. For example, 2′-deoxy substitutions are known to change the preferred sugar pucker from $C_{3'}$-endo to $C_{2'}$-endo (*24*). Another 2′-deoxy effect is the introduction of unoccupied space, formerly filled by the hydroxyl group, that may require local structural or solvent reorganization. It is impossible to know beforehand whether these effects will stabilize or destabilize tertiary folding of the RNA. For the 2′-deoxy derivatives, our data allow us to estimate the magnitudes of these side effects, because some of the multiple 2′-deoxy substitutions are redundant. For example, because the A184 2′-deoxy substitution disrupts both hydrogen bonds of the C109:A184 interaction, adding the C109 2′-deoxy substitution (as in the C109:A184 double mutant) does not delete any more hydrogen bonds. Therefore, comparing the $\Delta\Delta G^{\circ\prime}$ values for the A184 and C109:A184 2′-deoxy mutants reveals the combined side effects of the C109 2′-deoxy substitution other than hydrogen bond deletions.

For nucleotide C109, three derivatives are redundant: C109:A184 as compared with A184; C109:G110:A184 as compared with G110:A184; and C109:A183:A184 as compared with A183:A184. Using the values in Table 2, the differences in $\Delta\Delta G^{\circ\prime}$ for these three pairs are 0.1, 0.3, and −0.2 kcal/mol. That is, the C109 2′-deoxy substitution, in the context of the A184 2′-deoxy substitution, is worth only an additional 0.1 kcal/mol of destabilization. Similarly, the C109 2′-deoxy substitution in the context of G110:A184 is worth 0.3 kcal/mol of destabilization, and the C109 2′-deoxy substitution in the context of A183:A184 is worth 0.2 kcal/mol of *stabilization*. Therefore, the side effects of the C109 2′-deoxy substitution (independent of hydrogen bond deletions) contribute little, on average, to changes in the tertiary folding free energy of P4−P6.

For nucleotide A183, as for C109, three derivatives are redundant: G110:A183 as compared with G110; C109:G110:A183 as compared with C109:G110; and G110:A183:A184 as compared with G110:A184. The differences in $\Delta\Delta G^{\circ\prime}$ for these three pairs are 0.3, 0.3, and 0.7 kcal/mol. Thus, the A183 2′-deoxy substitution alone has, on average, more deleterious side effects than the C109 2′-deoxy substitution—0.3−0.7 kcal/mol of destabilization. One additional comparison, C109:G110:A183:A184 with G110:A184, estimates the combined effects of C109+A183 2′-deoxy substitutions; the difference in $\Delta\Delta G^{\circ\prime}$ is 0.7 kcal/mol. This is consistent with small C109 2′-deoxy side effects and more substantial A183 side effects.

2′-Methoxy Substitutions Have a More Complex Trend. We also studied the complete series of 2′-methoxy derivatives for the four nucleotides highlighted in Figure 1. Each 2′-methoxy substitution is expected to disrupt a single hydrogen bond regardless of substitution at partner I or II. The change in folding free energy $\Delta\Delta G^{\circ\prime}$ is plotted versus number of deleted hydrogen bonds for all 2′-methoxy derivatives in Figure 5B. Clearly the trend is quite different from the 2′-deoxy series—multiple 2′-methoxy substitutions do not contribute additively to $\Delta\Delta G^{\circ\prime}$. Perhaps the most striking result is that the quadruple 2′-methoxy derivative, with four deleted hydrogen bonds, has a $\Delta\Delta G^{\circ\prime}$ of approximately zero. That is, despite disruption of four hydrogen bonds, the $\Delta G^{\circ\prime}$

for the tertiary folding transition is approximately unchanged relative to wild-type P4−P6. Overall, the trend of $\Delta\Delta G^{\circ\prime}$ versus number of hydrogen bond deletions may be described as inverted-U-shaped, with the G110:A183 double 2′-methoxy derivative a relative outlier.

2′-Methoxy Substitutions at Other Positions. For controls, we chose four positions (U107, A114, G188, and C193) for which replacement of 2′-hydroxyls with 2′-methoxy substituents should not introduce any unfavorable interactions into P4−P6, according to visual inspection of the X-ray crystal structure (*3*). The $\Delta\Delta G^{\circ\prime}$ values for these four positions were 0.1, 0.0, 0.3, and 0.1 kcal/mol (data not shown). Only the third value is significantly different from zero, and this only marginally so. Therefore, the mostly larger $\Delta\Delta G^{\circ\prime}$ values tabulated in Table 2 probably reflect perturbation of specific folding interactions, not the simple addition of methyl groups to an RNA molecule.

We also examined a third P4−P6 ribose zipper interaction, C137/A186. This interaction is at the heart of the important A-rich bulge, and the A186U mutation is known to be particularly disruptive to P4−P6 folding (*25*). Therefore, one might expect significant disruption of folding with bulky 2′-substitutions at these positions. Indeed, substituting 2′-methoxy groups at either C137 or A186 gave very substantial effects (several kcal/mol) on the tertiary folding $\Delta G^{\circ\prime}$ (Table 2); the Mg^{2+} Hill coefficient for the C137 derivative may also be reduced relative to wild-type P4−P6 (see Supporting Information). We prepared the C137:A186 double 2′-methoxy derivative, but no discrete band migrating faster than P4−P6-bp was observed (data not shown). On the basis of not observing a folding transition at even 30 mM Mg^{2+}, we estimate the $\Delta\Delta G^{\circ\prime}$ for the C137:A186 double 2′-methoxy mutant as >9 kcal/mol. The 2′-deoxy derivatives at C137 and/or A186 have not yet been studied.

Temperature-Gradient Gels Separate Enthalpic and Entropic Contributions for the 2′-Methoxy Derivatives. The Mg^{2+} titrations allow computation of the folding $\Delta\Delta G^{\circ\prime}$s, but separating these $\Delta\Delta G^{\circ\prime}$s into enthalpic and entropic contributions requires a variable-temperature study. We selected the quadruple 2′-methoxy derivative (C109:G110:A183:A184, for which $\Delta\Delta G^{\circ\prime} \approx 0$) for such a study, using the previously reported temperature-gradient gel electrophoresis (TGGE) method (*18*). The quadruple 2′-methoxy derivative was chosen for two reasons. First, thermodynamic parameters determined from TGGE data are subject to significant experimental uncertainty, and we expected the largest thermodynamic perturbations with the greatest number of 2′-methoxy substitutions. Second, we consider that obtaining thermodynamic parameters at the same $[Mg^{2+}]/[Mg^{2+}]_{1/2}$ for different RNAs is critical for meaningful comparison of the results, because $\Delta H^{\circ\prime}$ and $\Delta S^{\circ\prime}$ values are known to depend on $[Mg^{2+}]$ (*18*). Because $\Delta\Delta G^{\circ\prime} \approx 0$ for the quadruple 2′-methoxy derivative, we could perform TGGE for both it and wild-type P4−P6 at the same absolute $[Mg^{2+}]$ of 0.65 mM ($\approx[Mg^{2+}]_{1/2}$), which allows sufficient resolution of the tertiary folding transition for each RNA. Because most any other 2′-methoxy (or any 2′-deoxy) derivative has a different $[Mg^{2+}]_{1/2}$ than wild-type P4−P6, interpretable TGGE data for these other RNAs would be much harder to obtain.

The TGGE experiments were performed essentially as described (*18*), and the electrophoresis patterns were qualitatively similar to those previously observed (data not shown). Three gels were run for both wild-type P4−P6 and the quadruple 2′-methoxy derivative, and representative van't Hoff plots are shown in Figure 6. For wild-type P4−P6, the thermodynamic values are $\Delta H^{\circ\prime} = -22.5 \pm 1.4$ kcal/mol and $\Delta S^{\circ\prime} = -71.8 \pm 4.3$ eu, whereas for the quadruple 2′-methoxy derivative, the values are $\Delta H^{\circ\prime} = -18.2 \pm 1.2$ kcal/mol and $\Delta S^{\circ\prime} = -58.0 \pm 3.5$ eu. Both the present and previous (*18*) study examine wild-type P4−P6 under buffer conditions where $[Mg^{2+}] \approx [Mg^{2+}]_{1/2}$. In the previous report, using a Tris-Hepes-Na^+ buffer instead of the presently used Tris-borate, at $[Mg^{2+}]_{1/2}$ the thermodynamic parameters were $\Delta H^{\circ\prime} = -28 \pm 3$ kcal/mol and $\Delta S^{\circ\prime} = -91 \pm 8$ eu. These values differ slightly from the ones reported above, which could be due to different buffer compounds (Tris versus Hepes) or the presence/absence of Na^+. Therefore, comparisons are restricted to our new data all obtained under the same conditions. These data show that the folding $\Delta H^{\circ\prime}$ for the quadruple 2′-methoxy derivative is less favorable (less negative) than for wild-type P4−P6. However, the folding $\Delta S^{\circ\prime}$ is *more* favorable (also less negative) for the quadruple mutant, consistent with hydrophobic effects due to multiple 2′-methoxy substitution. Thus, unfavorable enthalpic and favorable entropic effects combine to leave $\Delta G^{\circ\prime}$ approximately unchanged for the quadruple 2′-methoxy derivative.

Ribozyme Catalytic Activity is Not Much Affected by 2′-Deoxy Substitution but Is Significantly Reduced by 2′-Methoxy Substitution. Tetrahymena group I intron catalytic activity can be reconstituted by combining the P4−P6 and P3−P9 domains of the intron with the P1−P3 domain, which contains the 5′ splice site analogue (*19*). The catalytic competence of a P4−P6 derivative may be assayed in such a system by monitoring the cleavage rate of radiolabeled P1−P3. Using this three-piece catalytic activity assay, we examined the kinetic competence of two of the P4−P6 derivatives, the G110:A184 double 2′-deoxy derivative and the C109:G110:A183:A184 quadruple 2′-methoxy derivative. Each of these has all four ribose zipper hydrogen bonds of Figure 1 disrupted. The catalytic half-lives were determined at 50 mM Mg^{2+}, where both derivatives and the wild-type are completely folded by the native gel assay despite any energetic disruptions in the derivatives. At 25 °C and using 100 nM P4−P6, wild-type P4−P6 promoted cleavage of the P1−P3 substrate with half-life $t_{1/2} = 7.3 \pm 0.2$ min (three determinations). The double 2′-deoxy derivative had virtually the same catalytic activity, with $t_{1/2} = 8.4$ min (one determination). In contrast, the quadruple 2′-methoxy derivative had a noticeably reduced activity, with $t_{1/2} = 50 \pm 4$ min (two determinations). We raised the [P4−P6] from 100 to 500 nM to check if the substitutions affected the apparent K_m for P4−P6 binding. As expected, the wild-type was almost unaffected ($t_{1/2}$ lowered by only 9%), indicating that $K_m \ll 100$ nM as previously shown (*19*). The quadruple 2′-methoxy derivative was affected much more ($t_{1/2}$ lowered by 40%), indicating that the multiple 2′-methoxy substitutions affect both the catalytic activity and the domain binding ability of the P4−P6 subunit.

DISCUSSION

RNA tertiary folding is the conversion of a molecule with only secondary structure (base-paired helices and connecting

loops) to a molecule with a specific, more complex three-dimensional shape. A well-known example is the folding of the tRNA cloverleaf secondary structure into the L form observed by X-ray crystallography (*24*). To predict higher-order RNA folding and the effects of mutations on folding, one must know the energetic contribution of individual tertiary interactions, preferably observed at high resolution. Furthermore, one must know whether such interactions are independent of, or cooperative with, nearby interactions. In the present study, we systematically quantify the energetics and cooperativity of one set of "ribose zipper" tertiary hydrogen bonds in the *Tetrahymena* group I intron P4−P6 domain.

Estimated $\Delta G^{\circ\prime}$ Contributions of Individual RNA Hydrogen Bonds and of Ribose Zipper Teeth. The complete array of 2′-deoxy derivatives reveals that the four hydrogen bonds in the C109/A184 and A183/G110 ribose zipper motif each contribute only −0.4 to −0.5 kcal/mol to the tertiary folding $\Delta G^{\circ\prime}$ of P4−P6 (Figure 5A). Thus, each two-hydrogen-bond ribose zipper "tooth" contributes about −1.0 kcal/mol to $\Delta G^{\circ\prime}$. Although some of our values are slightly higher (−1.2 to −1.3 kcal/mol), correction for 2′-deoxy side effects would reduce them to ∼−1.0 kcal/mol per tooth. These values for $\Delta G^{\circ\prime}$ contributions can be compared with available literature estimates for proteins and for nucleic acid secondary and tertiary structures. For example, in a study of tyrosyl-tRNA synthetase, Fersht and co-workers found that nonionic hydrogen bonds contribute −0.5 to −1.5 kcal/mol to $\Delta G^{\circ\prime}$, while ionic hydrogen bonds are worth more (∼−3 kcal/mol) (*26*). Measurements of hydrogen bond strengths in nucleic acid secondary structures are around −0.5 to −1 kcal/mol per hydrogen bond (*27*), with an estimated maximum value of −2 kcal/mol (*28*). In the case of a stable GCAA tetraloop, hydrogen bonds appear to be worth only −0.2 to −0.7 kcal/mol (*29*). Few examples of RNA tertiary interactions have been quantified; in one instance, the binding free energy between the *Tetrahymena* intron and its guanosine substrate includes contributions of about −1.4 kcal/mol per hydrogen bond (*30*). Our value of −0.4 to −0.5 kcal/mol for an RNA tertiary hydrogen bond is therefore on the low side for known nonionic hydrogen bonds. In general, such deletion analysis provides a lower limit on RNA hydrogen bond strengths, because removal of one hydrogen bond may allow the structure to rearrange slightly, strengthening other interactions (*31*). However, in P4−P6 the tertiary folding transition is envisioned as the coming together of two quasi-helical subdomains, oriented by the tetraloop-receptor and A-rich bulge-minor groove interactions (*3*). With this type of folding, it is not clear what sort of local rearrangement could compensate for loss of a long-range hydrogen bond.

2′-Methoxy Substitutions Have Unfavorable Enthalpic and Favorable Entropic Effects. The 2′-methoxy mutations have a less straightforward effect on P4−P6 folding (Figure 5B). Single 2′-methoxy substitutions have a fairly large destabilizing effect ($\Delta\Delta G^{\circ\prime} \approx 1$ kcal/mol), but the trend does not continue with additional 2′-methoxy groups. Indeed, when four 2′-methoxy substitutions are made, the tertiary folding $\Delta G^{\circ\prime}$ is approximately unchanged relative to wild-type P4−P6. The overall trend for the 2′-methoxy series is inverted-U-shaped and *opposite* to that of the 2′-deoxy series when more than one hydrogen bond is deleted. What thermodynamic effects can explain these 2′-methoxy data? Aside from any enthalpic and entropic contributions which would be shared with 2′-deoxy substitutions, including hydrogen bond deletions, 2′-methoxy substitutions have two obvious other possible consequences: (1) unfavorable steric interactions (clashes) with positive $\Delta\Delta H^{\circ\prime}$ contributions and (2) favorable hydrophobic and/or packing interactions with positive $\Delta\Delta S^{\circ\prime}$ and/or negative $\Delta\Delta H^{\circ\prime}$ contributions. One would expect the magnitude of all of these effects to increase as more 2′-methoxy substitutions are introduced.

2′-Methoxy groups likely cause steric clashes (*32*) that explain the uniform ∼1 kcal/mol destabilization observed with single such substitutions. Because the derivatives with one hydrogen bond deleted by 2′-methoxy substitution are more destabilized than analogous 2′-deoxy derivatives ($\Delta\Delta G^{\circ\prime} \approx 1$ kcal/mol versus <0.5 kcal/mol, Figure 5A versus Figure 5B), steric interactions appear to be as important as individual hydrogen bond disruptions for single 2′-methoxy substitutions. However, steric effects are in the wrong direction to explain the stabilizing trend seen with multiple 2′-methoxy substitutions. We suggest that hydrophobic and/or packing interactions involving the newly introduced 2′-methoxy groups explain the observed trend in Figure 5B. More specifically, a hydrophobic effect occurs by transfer of a nonpolar group (in this case, a 2′-methoxy) from water into a less polar environment (proximity to the other 2′-methoxy group or groups). This liberates water molecules, giving a favorable positive entropy change. The G110:A183 double mutant appears to be an outlier relative to the other data points, and we speculate that the two 2′-methoxy groups are oriented particularly well for enthalpically favorable packing interactions in this molecule.

The TGGE data on the quadruple 2′-methoxy derivative show entropic effects that support this interpretation of hydrophobic interactions. The $\Delta S^{\circ\prime}$ term is more positive for the quadruple 2′-methoxy derivative than for wild-type P4−P6 (Figure 6), as expected for a straightforward hydrophobic effect. Thus, unfavorable 2′-methoxy steric interactions combined with hydrogen bond deletions likely explain the less negative $\Delta H^{\circ\prime}$ term for the quadruple 2′-methoxy derivative, but they are overwhelmed by entropically favorable hydrophobic interactions, and $\Delta G^{\circ\prime}$ is approximately unchanged. Hydrophobic effects are known to explain aspects of protein folding (*33*), and here we invoke similar effects in folding of a semi-synthetic RNA containing unnatural methyl groups.

Interpretation of Hydrogen Bond Deletions in Terms of Local Effects. All of the P4−P6 derivatives with 2′-deoxy or 2′-methoxy substitutions at nucleotides C109, G110, A183, and A184 are well behaved in the Mg^{2+}-dependent native gel assay (Figure 3). Therefore, we feel confident that the experimental $\Delta\Delta G^{\circ\prime}$ values reflect local hydrogen bond deletions, as opposed to some global folding disruption. Consistent with this view, the Hill coefficients for the Mg^{2+} titrations are approximately unchanged from the value of 4 for wild-type P4−P6. These latter observations also make it unlikely that the hydrogen bond deletions indirectly affect Mg^{2+}-binding sites elsewhere in P4−P6. Finally, control experiments show that the structurally nonperturbing U107, A114, G188, and C193 2′-methoxy substitutions have minimal effects on $\Delta G^{\circ\prime}$, supporting the view that the hydrogen bond deletions have primarily local effects.

Table 3: Tests for Cooperativity between Adjacent Ribose Zipper Teeth Using the 2′-Deoxy Substitution Data

first mutant		second mutant		$\Delta\Delta G^{\circ\prime}$	double mutant	
site	$\Delta\Delta G^{\circ\prime}$ [b]	site	$\Delta\Delta G^{\circ\prime}$ [b]	expected[a,b]	sites	$\Delta\Delta G^{\circ\prime}$ [b]
C109	0.4	G110	1.0	1.4	C109:G110	1.4
C109	0.4	A183	0.2	0.6	C109:A183	0.7
A183	0.2	A184	1.1	1.3	A183:A184	2.0
G110	1.0	A184	1.1	2.1	G110:A184	1.6

[a] Expected for the limiting case of zero cooperativity (strict additivity of $\Delta\Delta G^{\circ\prime}$ values for first and second single mutants). [b] kcal/mol.

The catalytic activity kinetic data are also consistent with our interpretations. The G110:A184 double 2′-deoxy derivative has a catalytic rate and K_m at high [Mg^{2+}] almost unchanged relative to wild-type P4−P6, despite four hydrogen bond disruptions which cause an unfavorable, positive folding $\Delta\Delta G^{\circ\prime}$. Therefore, it is extremely unlikely that the 2′-deoxy substitutions cause any global perturbation of the P4−P6 structure, because one would expect these to decrease the catalytic activity and/or shift the K_m for P4−P6. In contrast, the quadruple 2′-methoxy derivative has a significantly lower catalytic activity and a higher P4−P6 K_m, although its folding $\Delta G^{\circ\prime}$ is approximately unchanged. We surmise that introduction of 2′-methoxy groups disrupts the contact surface between P4−P6 and the other ribozyme domains, which not only increases the K_m but also prevents essential interdomain interactions and lowers the catalytic rate.

In proteins, site-directed mutations that create vacant interior space can be compensated by significant structural rearrangement (*34*). Structural reorganization has also been observed in RNA upon mutation (*31*). If such rearrangement occurs in our derivatives, we would underestimate the energetic contributions of the associated hydrogen bonds. However, the relevant protein mutations alter entire amino acid side chains, whereas we have deleted single 2′-OH functional groups that leave much smaller cavities. Unlike site-specific mutations, functional group deletions do not introduce new functional groups that could engage in fortuitous, compensating interactions. Therefore, while perturbations due to structural rearrangement cannot be ruled out, they are likely to be small in our system.

Independence of Ribose Zipper Hydrogen Bonds. Are ribose zipper hydrogen bonds cooperative or independent? If the hydrogen bonds stabilize the folded RNA in a cooperative manner, then the $\Delta\Delta G^{\circ\prime}$ values should be nonadditive, and one would expect Figure 5A to be curved. However, the plot displays no consistent deviation from linearity, indicating that these particular hydrogen bonds contribute largely independently to the tertiary folding $\Delta G^{\circ\prime}$.

A more rigorous, quantitative determination of cooperativity analyzes the additivity of $\Delta\Delta G^{\circ\prime}$ values for specific mutants. Relevant cooperativity comparisons extracted from the 2′-deoxy data are shown in Table 3. For the C109:G110 and C109:A183 derivatives, the additivity is excellent, indicating no cooperativity between adjacent ribose zipper teeth. These are the only two possible comparisons involving the C109 2′-deoxy substitution, for which we have direct evidence that 2′-deoxy side effects are minimal. For the remaining two comparisons, the $\Delta\Delta G^{\circ\prime}$ of the double derivative is either somewhat higher (A183:A184) or lower (G110:A184) than predicted by additivity. For A183:A184, nonzero A183 2′-deoxy side effects may distort the cooperativity comparison. For G110:A184, the double mutant's $\Delta\Delta G^{\circ\prime}$ is about 75% of that expected from strict additivity. This double mutation is the only one which nonredundantly disrupts all four hydrogen bonds of Figure 1, and thus it would be expected to show the largest possible cooperativity effect. In summary, of the four comparisons in Table 3, only one suggests any cooperativity at all, and this only slightly so. Taken as a whole, the data do not compel that there are generally cooperative interactions between adjacent ribose zipper teeth.

Conclusions. Our thermodynamic analysis implies that the C109/A184 and A183/G110 "ribose zipper" motif is best thought of as comprising noncooperative contributions from individual teeth, each contributing about −1.0 kcal/mol to the tertiary folding $\Delta G^{\circ\prime}$ through its two hydrogen bonds. The single hydrogen bonds each provide −0.4 to −0.5 kcal/mol to the tertiary folding $\Delta G^{\circ\prime}$, and they contribute to higher-order RNA folding as independent elements just as well as they do in zippers consisting of two adjacent teeth. While the energetics of the hydrogen bonds in the examined ribose zipper show little evidence of context effects, further experimentation is required to evaluate the generality of this conclusion. Nevertheless, because the individual tertiary hydrogen bonds studied here are simple ribose−base or ribose−ribose interactions and not necessarily part of any recognizable motif, we speculate that our energetic values may be characteristic of simple pairwise interactions that mediate RNA tertiary folding. Studies such as this will allow a better understanding of the various thermodynamic contributions that stabilize folded RNA structures.

ACKNOWLEDGMENT

We thank Christina Tucker for assistance with initial experiments; Anne Gooding for RNA oligonucleotide synthesis; Karen Goodrich and Elaine Podell for DNA oligonucleotide synthesis; Stephen Scaringe (Dharmacon Research) for discussions and for synthesis of RNA oligonucleotides; Kara Juneau, Daniel Harrington, Michael Jarstfer, other members of the Cech lab, Scott Siewert, and Andrew Feig for many helpful discussions; Elaine Podell for guidance on TGGE; Anne Gooding for providing T7 RNA polymerase; and Jamie Williamson (Scripps) and Dan Herschlag (Stanford) for discussions on the thermodynamic measurements.

SUPPORTING INFORMATION AVAILABLE

Nondenaturing gels of P4−P6 derivatives with monovalent ions; Hill coefficient determinations and sample Hill plots; and tabulation of $\Delta\Delta G^{\circ\prime}$ values with error estimates. This material is available free of charge via the Internet at http://pubs.acs.org.

REFERENCES

1. Serra, M. J., and Turner, D. H. (1995) *Methods Enzymol. 259*, 242−261.
2. Uhlenbeck, O. C., Pardi, A., and Feigon, J. (1997) *Cell 90*, 833−840.
3. Cate, J. H., Gooding, A. R., Podell, E., Zhou, K., Golden, B. L., Kundrot, C. E., Cech, T. R., and Doudna, J. A. (1996) *Science 273*, 1678−1685.

4. Ferré-D′Amaré, A. R., Zhou, K., and Doudna, J. A. (1998) *Nature 395*, 567−574.
5. Pley, H. W., Flaherty, K. M., and McKay, D. B. (1994) *Nature 372*, 68−74.
6. Bevilacqua, P. C., and Turner, D. H. (1991) *Biochemistry 30*, 10632−10640.
7. Herschlag, D., Eckstein, F., and Cech, T. R. (1993) *Biochemistry 32*, 8299−8311.
8. Jaeger, L., Westhof, E., and Michel, F. (1993) *J. Mol. Biol. 234*, 331−346.
9. McConnell, T. S., and Cech, T. R. (1995) *Biochemistry 34*, 4056−4067.
10. Costa, M., and Michel, F. (1995) *EMBO J. 14*, 1276−1285.
11. Narlikar, G. J., Khosla, M., Usman, N., and Herschlag, D. (1997) *Biochemistry 36*, 2465−2477.
12. Pley, H. W., Flaherty, K. M., and McKay, D. B. (1994) *Nature 372*, 111−113.
13. Grosshans, C. A., and Cech, T. R. (1991) *Nucleic Acids Res. 19*, 3875−3880.
14. Murphy, F. L., and Cech, T. R. (1993) *Biochemistry 32*, 5291−5300.
15. Moore, M. J., and Query, C. C. (1998) in *RNA-Protein Interactions: A Practical Approach* (Smith, C. W. J., Ed.) pp 75−108, Oxford University Press, Oxford.
16. Moore, M. J., and Sharp, P. A. (1992) *Science 256*, 992−997.
17. Basu, S., Rambo, R. P., Strauss-Soukup, J., Cate, J. H., Ferré-D'Amaré, A. R., Strobel, S. A., and Doudna, J. A. (1998) *Nat. Struct. Biol. 5*, 927−930.
18. Szewczak, A. A., Podell, E. R., Bevilacqua, P. C., and Cech, T. R. (1998) *Biochemistry 37*, 11162−11170.
19. Doudna, J. A., and Cech, T. R. (1995) *RNA 1*, 36−45.
20. Cate, J. H., Hanna, R. L., and Doudna, J. A. (1997) *Nat. Struct. Biol. 4*, 553−558.
21. Szewczak, A. A., and Cech, T. R. (1997) *RNA 3*, 838−849.
22. Murphy, F. L., Wang, Y.-H., Griffith, J. D., and Cech, T. R. (1994) *Science 265*, 1709−1712.
23. Laggerbauer, B., Murphy, F. L., and Cech, T. R. (1994) *EMBO J. 13*, 2669−2676.
24. Saenger, W. (1984) *Principles of Nucleic Acid Structure*, Springer-Verlag, New York.
25. Murphy, F. L., and Cech, T. R. (1994) *J. Mol. Biol. 236*, 49−63.
26. Fersht, A. R., Shi, J.-P., Knill-Jones, J., Lowe, D. M., Wilkinson, A. J., Blow, D. M., Brick, P., Carter, P., Waye, M. M. Y., and Winter, G. (1985) *Nature 314*, 235−238.
27. Freier, S. M., Sugimoto, N., Sinclair, A., Alkema, D., Neilson, T., Kierzek, R., Caruthers, M. H., and Turner, D. H. (1986) *Biochemistry 25*, 3214−3219.
28. Turner, D. H., Sugimoto, N., Kierzek, R., and Dreiker, S. D. (1987) *J. Am. Chem. Soc. 109*, 3783−3785.
29. SantaLucia, J., Jr., Kierzek, R., and Turner, D. H. (1992) *Science 256*, 217−219.
30. Bass, B. L., and Cech, T. R. (1984) *Nature 308*, 820−826.
31. Jucker, F. M., Heus, H. A., Yip, P. F., Moors, E. H., and Pardi, A. (1996) *J. Mol. Biol. 264*, 968−980.
32. Narlikar, G. J., and Herschlag, D. (1996) *Nat. Struct. Biol. 3*, 701−709.
33. Kellis, J. T., Jr., Nyberg, K., Sali, D., and Fersht, A. R. (1988) *Nature 333*, 784−786.
34. Xu, J., Baase, W. A., Baldwin, E., and Matthews, B. W. (1998) *Protein Sci. 7*, 158−177.

BI9906118